Calculation of CO2 column heights in depleted gas fields from known pre-production gas column heights

Calculation of CO_2 column heights in depleted gas fields from known pre-production gas column heights

M.Naylor, M.Wilkinson and R.S.Haszeldine

School of GeoSciences, University of Edinburgh, EH9 3JW.

Corresponding author: Mark Naylor, email: mark.naylor@ed.ac.uk

Abstract

Depleted gas fields have been identified as potential targets for CO_2 storage. In order to maximise storage capacity, a target field must be deep enough to ensure that the CO_2 is in a dense phase (either liquid or supercritical). Accurate assessment of the storage capacity also requires an estimation of the amount of CO_2 that can be safely stored beneath the reservoir seal which can be estimated in several ways. In this paper we develop a methodology to convert known pre-production gas column heights into CO_2 column heights in order to estimate storage capacities. Several authors have correctly identified that the differences in interfacial tension and wettability act to reduce the threshold capillary entry pressure for CO_2 compared to natural gas, consequently reducing column height estimates. However, under reservoir conditions the density of CO_2 is substantially higher than natural gas so the buoyancy force on the seal for a fixed column height is much lower for dense phase CO_2 increasing column height estimates; we investigate the effects of this trade off on storage estimates and apply it to a typical dataset, in this case the UK North Sea.

Keywords: Carbon dioxide storage, capacity, gas fields, column height

1 Introduction

Depleted gas fields are good contenders for engineered CO_2 storage, having both proven seals and well characterised geology. Assessment of the suitability of a field for CO_2 storage requires the estimation of storage capacity. The most simplistic approach assumes volume-for-volume replacement, with a discount factor for water invasion into the storage zone [*S Bachu and J Shaw*, 2003].

The physical properties of CO_2 differ from those of hydrocarbon gas, so that there is the possibility that capillary seals which are secure for hydrocarbons will not be secure for CO_2. A number of authors have highlighted that the differences in interfacial tension (IFT) and wettability between CO_2 and natural gas act to reduce the threshold capillary entry pressure for CO_2 compared to gas, reducing storage estimates [e.g. *P Chiquet et al.*, 2007a; *P Chiquet et al.*, 2007b]. However, for cases with good hydraulic connectivity to the aquifer, the full assessment of the storage capacity beneath a capillary seal also requires knowledge of the buoyancy drive exerted on the seal by the stored fluid. Since the density of dense phase CO_2 is substantially greater than that of natural gas under reservoir conditions, a column height of CO_2 exerts a lower buoyancy drive on the seal than the same column height of natural gas. Thus, the phase behaviour of CO_2 counteracts the reduction in capillary entry pressure. This balance between entry pressures and buoyancy, and the conversion of gas column heights to CO_2 column heights is the topic of this paper.

Our approach is to take the known, pre-production column height of natural gas within a reservoir and use the known differences in material properties between the original gas and the stored CO_2 to convert the pre-production natural gas column height to a safe CO_2 column height. The advantage of this technique is that it does not require knowledge of intrinsic properties of the seal, such as the effective (maximum) pore throat radius, which are generally unknown and have very large uncertainties. It requires that the drive on production was primarily hydraulic so that we can assume the force on the seal due to the presence of CO_2 can be expressed as buoyancy derived from displacing formation water. Our terminology is hence as follows:

- Pre-production column height – the column height corresponding to the reserves of gas in the trap prior to extraction which may be capillary limited or may be limited by a spill-point or by gas supply in the case of an under filled field.

- Maximal CO_2 column height –This is the upper bound on the CO_2 column height estimate and is calculated from the pre-production gas column height taking into account buoyancy and interfacial tension differences between natural gas and CO_2, both properties that are relatively well characterised. Thus, this estimate is purely a function of the material properties of CO_2 and natural gas. Where the natural gas field was capillary limited, the calculated maximal CO_2 column height corresponds to the point where the buoyancy pressure of the CO_2 equals (actually is infinitesimally less than) the entry pressure of the seal such that the seal would leak by capillary failure.
- Safe CO_2 column height - the maximal column height neglecting the mineralogical dependent effects of contact angles on the column height estimate. Depending upon the mineralogy of the seal, the inclusion of contact angles will reduce the column height estimate. This term has experimental, upscaling and theoretical uncertainties.
- Column height conversion factor (□)– the ratio of the pre-production natural gas column height to the CO_2 column height. In this paper a methodology is developed to calculate this value from typical hydrocarbon field data. Conversion factors of less than 1 indicate a reduction of the CO_2 column height compared to the gas column height. This term can also be prefixed with safe or maximal to describe whether contact angles are taken or are not taken into account respectively.

The structure of this paper is to first develop the theory behind the calculation of CO_2 column heights from gas column heights identifying a conversion factor, next we investigate the controls on that conversion factor, then a discussion informed by typical data and finished off with a discussion of some secondary, related effects.

2 Column height conversion factor - capillary model

Across a curved interface between two immiscible fluids a discontinuity in fluid pressure occurs as a consequence of the interfacial tensions at the interface. The capillary pressure, P_c is the difference in pressure between a non-wetting phase, p_{nw} and a wetting phase, p_w,

$$P_c = p_{nw} - p_w \quad . \quad (1)$$

The seal is usually a very tight porous material, typically imbibed with water, beneath which the hydrocarbon or CO2 sits in a more porous and permeable reservoir rock. The threshold pressure, P_{th}, marks the point above which the non wetting phase (here, the hydrocarbon gas or CO2) displaces the (typically) water phase that imbibes the seal; in terms of basic physics it is the value at which the pressure gradient in both phases becomes continuous. The pressure where a phase first starts to enter a caprock is referred to as the entry pressure (limited by the largest pore throat at the reservoir-caprock interface) and the pressure where a phase can travel through the entire thickness of the caprock is the breakthrough pressure and is generally slightly larger than the entry pressure (limited by the largest pore throat in the least resistance pathway through the caprock). We assume the capillary threshold pressure to be the limiting factor controlling the amount of stored natural gas or CO_2 in the systems considered here. Other first order controls of a column height may include being filled to a structural spill point, formation reworking or that the trap is under-filled because of a finite supply of hydrocarbon charge. The threshold capillary pressure, $P_{c,th}$ is controlled by the surface tension between the two fluids (γ), the contact angle in the wetting phase (i.e. water) with the caprock (θ_{seal}) and reservoir (θ_{res}) as well as the geometrical properties of the pore network in the seal and reservoir (described by r_p and r_t or combined in an effective pore radius, R),

$$P_{c,th} = \gamma\left(\frac{\cos\theta_{seal}}{r_t} - \frac{\cos\theta_{res}}{r_p}\right) \approx \frac{\gamma\cos\theta}{R} \quad . \quad (2)$$

where r_p and r_t are the pore and throat radii respectively. The contact angle arises as a surface chemistry effect and is therefore a function of the rock as well as the two phases; it is close to zero when the substrate is strongly water-wet.

It follows that the threshold pressure, or displacement pressure, P_{th}, in the non-wetting phase is equal to $P_w + P_{c,th}$, where P_w is the pressure in the water (or brine) phase, often equal to the hydrostatic pressure.

Since the limiting pore and throat radii are impossible to measure directly, a common way to proceed is to estimate the pore throat radii using a porosity-permeability relationship [e.g. *R R Berg*, 1975; *S Bloch*, 1991; *M R Rezaee et al.*,

2006]. For example, an effective grain size, D_e can be calculated from core analysis using an empirical permeability equation such as $D_e = \left(1.89\, k\, n^{-5.1}\right)^{0.5}$ [cm], where k is the permeability [mD] and n is the porosity [percent] [*R R Berg*, 1975]. The pore and throat sizes can then be estimated using D_e and assuming a theoretical packing geometry. In a rhombohedral packing with perfect spheres $r_p = 0.5 \times 0.414 D_e$ and $r_t = 0.5 \times 0.154 D_e$. Whilst this may practically be the only way forward for an exploration scenario, it is susceptible to large uncertainties in upscaling from sparse core samples to the whole reservoir and the predictive capability of any such empirical relationship is strongly limited by the calibration data.

The buoyancy pressure exerted on the seal due to a column of height, h of less dense fluid under hydrostatic conditions is simply given by,

$$P_b = \Delta\rho g h \quad . \quad (3)$$

Where $\Delta\rho$ is the absolute density difference and g the acceleration due to gravity.

Equating the pressures in Eqns (2) and (3), the capillary limited column heights for the gas/water can be expressed as,

$$\frac{\gamma_{gas/water} \cos\theta_{gas/water}}{R} = \Delta\rho_{gas/water}\, g\, h_{gas/water} \quad . \quad (4)$$

We can construct the analogous equation for the CO_2/water systems as for the gas/water system in (4),

$$\frac{\gamma_{CO2/water} \cos\theta_{CO2/water}}{R} = \Delta\rho_{CO2/water}\, g\, h_{CO2/water} \quad . \quad (5)$$

The geological factor in equations (4) and (5) is the pore geometry, expressed in the term R. This is an unknown factor in almost all storage settings, but can now be simply removed from further consideration. Utilising the fact that both fluids interact with the same pore geometry, we can divide (4) and (5) to remove this term. This gives us an expression for the CO_2 column height as a function of the measured gas column height and physical/chemical properties of the fluid-rock systems.

$$h_{CO2/water} = h_{gas/water} \frac{\Delta\rho_{gas/water}}{\Delta\rho_{CO2/water}} \frac{\cos\theta_{CO2/water}}{\cos\theta_{gas/water}} \frac{\gamma_{CO2/water}}{\gamma_{gas/water}} \quad . \quad (6)$$

This gives the conversion ratio for gas/water column heights to CO_2/water column heights as,

$$\psi_{gas/CO2} = \frac{\Delta\rho_{gas/water}}{\Delta\rho_{CO2/water}} \frac{\cos\theta_{CO2/water}}{\cos\theta_{gas/water}} \frac{\gamma_{CO2/water}}{\gamma_{gas/water}} \quad . \qquad (7)$$

Thus, the conversion factor is a combination of the ratios of the density differences, contract angles and interfacial tensions for the gas/water – CO_2/water systems. We discuss each of these key ratios in turn.

2.1 Interfacial Tension (IFT) ratio

At the reservoir/seal boundary, the IFT between the wetting and non-wetting fluids linearly increases the capillary entry pressure that must be overcome in order for the wetting fluid to invade the seal. The IFT for hydrocarbon/water systems has been used extensively for many years in the industry and has been extensively characterised. We use methane as an example here because it is at the upper limit of hydrocarbon IFTs and is thus provides a worst case scenario for the effects of this term. The IFT for CO_2/water systems has not been investigated as extensively and consensus regarding its behaviour is only just starting to emerge [*P Chiquet et al.*, 2007b; *Q Y Ren et al.*, 2000]. For both methane-water and CO_2-water, the IFTs increase rapidly at low pressures but become increasingly stable with increasing pressure (Figure 1). As an approximation, we can take the ratio at 10MPa as representative of typical reservoir depths where $\gamma_{CO2/water} \approx 25$ mN/m [*P Chiquet et al.*, 2007b] and $\gamma_{CH4/water} \approx 50$ mN/m [*A Danesh*, 2007; *Q Y Ren et al.*, 2000]. This gives an IFT ratio ~ 0.5.

The effect of the IFT ratio term is to lower the capillary entry pressure for pure CO_2/water systems by up to 50 % compared to the pure gas/water system [*Z W Li et al.*, 2006]. Thus the effect of this term is to decrease the maximum column height of CO_2 relative to the methane gas column height.

The methane-water system that existed prior to CO_2 injection may have contained significant CO_2, and this must be accounted for in calculating the change in IFT due to CO_2 injection. It has been experimentally demonstrated that in mixtures of CO_2 and methane, higher proportions of CO_2 reduce the IFT [*Q Y Ren et al.*, 2000], consistent with the CO_2 IFT being lower than that of methane. However, Chiquet et al [2007b] demonstrated that previous analysis of the CO_2/water IFT values was biased towards lower values as previous workers had assumed an incorrect density for the CO_2 saturated water phase. Figure 1 shows a compilation of data for the (CO_2+CH_4)/water system. We choose to linearly interpolate between the pure

methane/water and CO_2/water IFT values, consistent with this observation, since there is not sufficient data to do better .

Thus we suggest a correction to the ratio that accounts for known amounts of CO_2 in the original gas. We define the mol% of CO_2 in the natural gas as x_{CO2} and CH_4 as x_{CH4}. Using this we estimate the IFT of the natural gas / water system,

$$\gamma_{gas/water} \approx x_{CO2}\gamma_{CO2/water} + x_{CH4}\gamma_{CH4/water} \approx x_{CO2}\gamma_{CO2/water} + (1 - x_{CO2})\gamma_{CH4/water} \quad (8)$$

Therefore, the ratio of the IFTs is given by

$$\frac{\gamma_{CO2/water}}{\gamma_{gas/water}} = \frac{\gamma_{CO2/water}}{x_{CO2}\gamma_{CO2/water} + (1 - x_{CO2})\gamma_{CH4/water}} = \frac{1}{x_{CO2} + (1 - x_{CO2})\dfrac{\gamma_{CH4/water}}{\gamma_{CO2/water}}} \quad (9)$$

$$\approx \frac{1}{2 - x_{CO2}}$$

The ranges of this ratio are from 0.5 if the natural gas was pure methane (i.e. $x_{CO2} = 0$) to 1 in the (unrealistic for our purposes) end member that the natural gas was initially pure CO_2 (i.e. $x_{CO2} = 1$).

2.2 Density difference ratios

The density difference ratio describes the relative difference in the buoyancy drive between the CO_2/water and natural gas/water systems. Since buoyancy in the subsurface is generally derived from displacing formation water, this approach is appropriate for systems with good hydraulic connectivity to the aquifer. This buoyancy force provides the drive that must overcome the capillary entry pressure if the non-wetting fluid is to invade the caprock. The greater the buoyancy contrast, the stronger the drive.

We demonstrate typical subsurface buoyancy depth profiles using two end-member subsurface scenarios corresponding to different heat flow regimes and sub-aerial and submarine conditions (Figure 2).

We calculate pressure P, temperature T and salinity w_s as a function of depth from defined surface pressure, temperature and salinity values and corresponding geothermal, hydrostatic gradients and salinity gradients. Salinity tends to increase with depth from sea water concentrations offshore and freshwater concentrations onshore [*Moss, B. et al.*, 2003]; the salinity gradient is highest when salt layers are

present in the subsurface (e.g. Southern North Sea). These profiles are then used to calculate how the phase properties of CO_2, natural gas and water vary with depth. We define the depth, z to be the distance beneath the surface, which corresponds to either the topographic elevation or the seafloor. In the submarine case, the surface pressure also includes the pressure exerted by the water above the seabed.

These calculations are typically conditioned to initial reservoir conditions and neglect coupled processes associated with the injection of CO_2 which requires a full reservoir simulation. They are useful for the rapid initial assessment of a wide range of storage scenarios and should be used in conjunction with geological and hydrodynamic information (such as the water drive) to identify which coupled processes will be important for each specific target. Thus this methodology provides a technique for the preliminary site assessment prior to a more complete analysis using reservoir simulations.

We use standard calculations (See appendices) to determine the densities of the fresh (where $w_s = 0$) and saline formation water, $\rho_w(P,T,w_s)$, the produced gas (assuming a specific gravity of 0.65 and a compressibility factor of 0.85), $\rho_{gas}(P,T,M_{gas})$ and the injected CO_2, $\rho_{CO2}(P,T)$. The form of the density profiles all trade off between increases in pressure that tend to increase densities and increases in temperature which tend to decrease densities. We assume that the density will be fairly constant in the column which is reasonable when CO_2 persists in the dense phase or for relatively short column heights; for a full treatment on real data this assumption can be relaxed by integrating over an actual column. We neglect the effects of dissolution of CO_2 in the formation water as the small increase in saturate brine density is second order to the main effects described here.

The CO_2 vapour pressure curves are plotted with pressure-temperature pairs through the subsurface in Figure 2(a,b). In Case 2, where the pressure-temperature path crosses the vapour pressure curve, a phase transition from the gas to liquid phases is predicted at depths less than ~300m below the seabed (the depth corresponding to the critical pressure for CO_2); this is higher than would be expected for a sub-aerial case because of the higher surface pressure which is site specific because of the dependency upon the water depth. For a range of realistic parameterisations, the density in the supercritical phase actually increases with shallower depths, acting to decreasing the buoyancy drive. In contrast, in Case 1

which corresponds to higher heat flow and lower surface pressure (sub-aerial) the pressure-temperature path does not intersect the vapour pressure curve and the predicted CO_2 densities correspond to a smooth trajectory from the supercritical density to gas densities over a much wider depth range always increasing the buoyancy drive.

In contrast to the CO_2 density profiles, the natural gas and water density profiles (Figure 2i,j) are better behaved as they are in more stable regions of their respective phase spaces. The formation water density is considerably less variable with typical values in the range 960 – 1030 kg/m^3 for fresh water and upto 1200 kg/m^3 for saline water with 25 % weight percent of salt dissolved.

Using these density profiles we calculate the density differences (Figure 2g,h) and density difference ratios (Figure 2i,j) which is the key controlling ratio that characterises the relative buoyancy drive

$$\frac{\Delta\rho_{gas/water}}{\Delta\rho_{CO2/water}} = \frac{\rho_{water} - \rho_{gas}}{\rho_{water} - \rho_{CO2}}$$

Whilst we chose end-members here, it should be noted that relatively subtle changes in the thermal and pressure regimes propagate through to a significant differences in the density difference profiles (Figure 2g,h), and corresponding predictions of the buoyancy drive. In the subsurface, the density of CO_2 is always greater than that of typical natural gas compositions. Since $\Delta\rho_{CO2/water}$ is lower than $\Delta\rho_{gas/water}$; the density difference term in the conversion factor increases the potential CO_2 column height. The density difference ratio is always greater than ~2 when CO_2 is in the dense phase and greatest when the pressure-temperature profile produces a phase change. The density of liquid phase CO_2 is nearly always higher than that in the supercritical phase, so we expect the safe CO_2 column height to be greater for subsurface conditions that encourage a phase change in the depth profile, i.e. cooler (lower surface temp and geothermal gradients) and submarine (higher surface pressure).

Since the typical minimum for the IFT ratio is 0.5, the buoyancy term should always at least counteract the decrease in column height due to the IFT effect for regions where CO_2 is in the dense phase.

Understanding the variation in CO_2 density with depth is key to determining the conversion factor and the degree to which the decreased buoyancy compensates

for the lower IFT in the CO_2/water system. Factors which increase the likelihood of being in a phase change regime are; lower geothermal gradients, lower surface temperatures and higher surface pressures, i.e. moving the well head pressure and temperature towards the top left in Figure 2 (a,b). Factors which decrease the likelihood of being in a phase change regime are; higher geothermal gradients, higher surface temperatures and lower surface pressures. The density of CO_2 at depths corresponding to pressures and temperatures near either the vapour pressure curve or the critical point will be subject to very high uncertainties and propagate through to high uncertainties in the conversion factor.

2.3 Contact angle ratio

The contact angle is the angle at which a liquid/vapour interface (here either hydrocarbon/water or CO_2/water) meets the solid surface (the surrounding rock). Contact angles arise from surface chemistry effects. This effect cannot be easily eliminated because the interaction of natural gas with a specific rock mineralogy does not necessarily act as a proxy for how CO_2 will behave; scaling from mineral scale experiments to core scale to reservoir scale is difficult. We need to know the contact angles for both the CO_2/water and gas/water systems for a given mineralogy in order to make the best estimate. CO_2 wettability is a complex story and a clear picture has not yet emerged as to the importance of wettability effects [*Chiquet et al.*, 2007a ; *Hildenbrand et al.*, 2004; *Li et al.*, 2005; *Yang et al.*, 2008].

The quantity of interest is the ratio of the cosines of both contact angles, which is hard to constrain precisely, but will be $\frac{\cos\theta_{CO2/water}}{\cos\theta_{gas/water}} \sim 1$. Given an initial water wet gas/water system, it will be less than 1.

Since there is a range of uncertainty in the contact angle of the CO_2/water system, we prefer to report a range of conservative (termed “safe”) and optimistic (termed “maximal”) values. The uncertainty in this term is significantly less than the uncertainty in the pore radius term R which contained order of magnitude uncertainty.

In the presence of the hydrocarbon phase, many minerals will generally be water wet giving a contact angle of 0^o giving a contribution to the denominator of the ratio of $\cos(\theta_{gas/water}) = \cos(0) = 1$. The use of this value provides the maximal CO2 column

height conversion factor. The presence of dense phase CO_2 has been shown to alter the water-wettability of various organic materials present in the subsurface, such as coal, resulting in an increase in the contact angle. Many seals are more-or-less organic-rich mudrocks (e.g. 5-10% organic content for the Kimmeridge Clay [*S Brown*, 1984]) so that the behaviour of this component of the rock is of potential importance.

In contrast, laboratory studies of contact angles [*P Chiquet et al.*, 2007a] backed up by breakthrough studies [*A Hildenbrand et al.*, 2004; *S Li et al.*, 2005] suggest that the presence of mica and quartz, minerals commonly present in shaley caprocks, reduce the contact angle ($\cos\theta \approx 0.66, \cos\theta \approx 0.85$ respectively). Espinoza and Santamarine [2010] look at contact angles in a range of systems; they show that for the contact angles are relatively pressure independent on quartz ($\cos\theta_{water/CO2} \approx 0.93$ and $\cos\theta_{brine/CO2} \approx 0.77$) and calcite ($\cos\theta_{water/CO2} \approx \cos\theta_{brine/CO2} \approx 0.77$). Since these angles were measured on pure samples, and real rocks are composed of a range of minerals, they too provide a conservative estimate for estimation of the safe CO2 column height conversion factor. The scaling of contact angles from a single mineral to multi-mineral reservoir is a non-trivial problem.

A CO2 storage study for the Rousse depleted gas field in France [*N. Tonnet et al.*, 2010] has analysed slices of the calcite and quartz rich caprock substrate, which is low in mica, and show it to remain water wet in the presence of CO_2.

A close look at the work by Chiquet et al. (2007a) shows that the water-wettability of quartz is barely altered in the presence of dense phase CO_2, as opposed to light phase CO_2 (see Fig. 8 in Chiquet et al., 2007a), whereas the contact angle values obtained with mica indicate that mica is becoming less water-wet when the CO_2 gets denser (i.e., pressure increases), even though there seems to be a strong dispersion in the contact angle values (see Fig. 7 in Chiquet et al., 2007a). With mica, less definitive conclusions were drawn in a subsequent study by the same laboratory [*Shah et al.*, 2008a].

The most conservative approach is to assume that the seal was completely water wet in the presence of the hydrocarbon and to use the most extreme reduction factor of 0.7. The most optimistic approach is to assume that the caprock will remain completely water wet, corresponding to a contact angle ratio of 1.0. Here we report the results of calculations for both scenarios.

3 Southern North Sea Example

We have applied this analysis to gas fields from the UK Southern North Sea, as a uniform publicly available dataset is available that includes gas expansion factors that are not otherwise commonly published, and chemical analyses of the gas [*I L Abbotts*, 1991]. The fields all contain dry gas, with methane contents of 91 – 95 mol %, and CO_2 contents of 0.4 – 1.2 mol % (Table 1). The seal in this instance is the Zechstein halite, so that capillary leakage is impossible, and the column height ratios would not need to be calculated in as real-life assessment of storage capacity. However, it does provide a realistic reference dataset for global submarine reservoir conditions that are also relevant to a number of cases where capillary leakage is the limiting factor; results on commercial datasets where capillary leakage is likely to be the limiting control are comparable. A histogram of the maximal and safe column height ratios calculated for these data is shown in Figure 3 for all the fields with sufficient information (Table 1).

The maximal column height ratios, neglecting contact angle changes, are all greater than 0.995 and less than 2. When experimental contact angles are included, the safe conversion factors are in the range of 0.7 – 0.92; the exceptions being the North and South Sean fields. In the latter, the predicted CO_2 densities are higher than other fields because the CO_2 is in the liquid phase with a density that is substantially higher than the supercritical CO_2 in the higher pressures and temperatures examples.

The conversion factor is more sensitive to changes in the CO_2 density than the gas density because the density difference between the CO_2 and water is smaller. The fields with the poorest conversion factors correspond to hot, low pressure reservoirs where the CO_2 is less dense, such as Ravenspurn South.

The above analysis indicates that the results of this assessment are crucially dependant upon the wetting behaviour of minerals in a CO_2-rich setting. It is suggested that more research is required in this field.

Where the conversion factor is confidently assessed as greater than 1, a further assessment of the structural geometry of the traps could be performed to assess whether any extra storage volume would be gained by an increased column height, i.e. filling any under-filled structures to spill point, subject to pressure increase limitations that are outwith the scope of this paper. If the safe column height conversion factors are taken to be the more realistic of the values calculated here, then this leads to a reduction in the CO_2 storage volume estimate of the fields. In geometrically complex

reservoirs, each trap requires individual assessment to calculate the storage capacity with the safe CO_2 column height.

In order to calculate the safe and maximal column heights, we multiply the conversion factors by the pre-production gas column height. Where the gas column was capillary limited, the CO_2 column heights are also capillary limited. However, the pre-production column height might not have been capillary limited. In an under filled gas field, the derived CO_2 column height will be a lower estimate of the true capillary limited capacity. Similarly, where the gas field is actually limited by a structural spill point, the derived CO_2 column height will also be a lower estimate.

This analysis has not taken into account irreversible invasion of water during the production phase which does not affect the estimate of the safe column height since buoyancy is purely derived from the vertical extent of a connected stringer of the buoyant fluid within the reservoir. However, the irreversible water saturation does affect the assessment of capacity, which is beyond the scope of this paper. Capacity is reduced by the irreversible invasion of water since it decreases the proportion of pore space available for CO_2 compared to what was available for the initial gas in place.

4 Second order factors

4.1 Effect of brine salinity on IFT

Thus far, we have not considered the effect of brine salinity on the IFT, the data in Figure 1 was for low salinity cases. The effects of brine salinity on measurements of IFT and wettability for the geological storage of CO_2 have been investigated by several authors [Aggelopoulos, 2010; Chalbaud et al., 2009; Espinoza and Santamarina, 2010; Massoudi and King, 1975]. They came to several important conclusions. Firstly, the basic form of the IFT curve is controlled primarily by the density difference between the CO_2 and brine. Further, increasing salinity linearly shifts the IFT curve to higher values at around a gradient of 1.3 mN/m per molal salt concentration. For salt concentrations above 30g/L of NaCl they found that the induced IFT increase was outwith experimental error.

This effect alone has the potential to increase the IFT in saline formations at depths where CO_2 would be in the dense phase by ~4-5 mN/m making the ratio,

$$\frac{\gamma_{CO2/brine}}{\gamma_{CH4/water}} \approx 3/5 = 0.6$$

compared to ~0.5 for the pure water case. However, increasing salinity can also increases the IFT for light hydrocarbon/water systems [e.g. Cai et al., 1996], which would moderate the potential increase. The effect of brine salinity on the IFT ratio is therefore generally a second order feature.

A comprehensive description of the effect of brine salinity on the hydrocarbon/brine IFT is a complicated problem due to the diversity of the composition of hydrocarbon phases. The salinity of the brine increases the IFT between the brine and either a gas or non-polar oil. However, polar fractions such as resins and asphaltenes may contain groups that tend to decrease the IFT. The magnitude of these effects will be on the same order as the effects CO_2 saturation in the brine.

Yang et al. (2005) measured the dynamic contact angle between CO_2, brine and crude oil systems. They noted that the measured dynamic IFT rapidly decays to a constant value explained by the absorption of CO_2 molecules and the reorientation of water molecules at the interface. CO_2 dissolution is also a factor with the crude oil. The IFTs are slightly lower in the presence of CO_2. These effects are pressure and temperature dependent.

4.2 Generalisation to sour-gas systems

Thus far, this paper has concentrated on the geological storage of CO_2 in a depleted field which contained either a pure hydrocarbon mixture or a hydrocarbon + CO_2 mixture. Now we include a brief discussion on how this system can be generalised to include H_2S in the predominantly CO_2 injection stream. Technically, an acid gas is any gas that contains significant amounts of acid gases such as CO_2 or H_2S; a sour as is a natural gas that specifically contains significant amounts of H_2S. Many of the fields yet to be developed contain sour gas and the disposal of H_2S is problematic. The conventional process is to separate the sulphur using the Claus process but, as well as several environmental challenges regarding this process, the production of sulphur by this mechanism is already in excess of world demand. An alternative way to deal with the H_2S is to reinject it into the subsurface, potentially mixed with CO_2, as part of a CCS project which is the context we are interested in here. Here we explore briefly how the terms of Eqn (7) would be altered by the presence of H_2S.

The wettability alteration induced by H_2S has been investigated on several substrates [Shah et al., 2008a]; it was found that with quartz and a caprock sample no significant wettability alteration was observed. With a mica substrate the water wettability was moderately altered in the presence of gaseous H_2S, and drastically in the presence of dense (liquid) H_2S.

The density of H_2S+CO_2 mixtures has to be considered in place of the density of pure CO_2 in the density difference ratio; data and models exist for predicting this density [e.g., C. E. Stouffer et al., 2001].

In order to estimate the impact of H_2S on CO_2 storage in a depleted gas field, we need to be able to assess the impact of H_2S on the IFT of gas mixtures. Pure H_2S has a lower IFT than either methane or CO_2 at approximately 20% of the pure methane value. It has been shown that we can estimate the IFT of mixtures including H_2S, by generalising the gas/water IFT estimation (Eqn 8) [*Shah et al.*, 2008b],

$$\begin{aligned}\gamma_{gasMixture/water} &\approx x_{H2S}\gamma_{H2S/water} + x_{CO2}\gamma_{CO2/water} + x_{CH4}\gamma_{CH4/water} \\ &\approx \left(0.2\,x_{H2S} + 0.5\,x_{CO2} + x_{CH4}\right)\gamma_{CH4/water}\end{aligned} \qquad (10)$$

As before, the influence of the IFT from different components is dependent upon the mole fraction of that component in the multi-component mixture. Thus the impact of the addition of a finite number of moles of H_2S on the IFT of the mixture is dependent on the absolute number of moles of the other components through the calculation of mole fractions.

We consider the implications for the range of likely storage scenarios involving a sour gas stream. There are a number of different sour-gas injection scenarios relevant to CO_2 storage; (i) injection of pure CO_2 into a field which initially contained a sour gas, (ii) injection of a CO_2 + H_2S mixture into a field which initially contained low amounts of H_2S, and (iii) injection of a CO_2 + H_2S mixture into a field which initially contained a sour gas.

4.2.1 Case (i): The initial gas in place was sour

The IFT of the initial gas in place would be lower than for a pure hydrocarbon gas resulting in the pre-production column height being lower than it would have been for a purer hydrocarbon, assuming that the capillary entry pressure of the seal was the limiting factor in determining the pre-production column height. Essentially, the reduced seal performance due to the presence of H_2S is recorded in the pre-production column height. For a known gas composition, the IFT of this pre-production mixture

can again be estimated using Eqn 10 and applied in Eqn 6 to convert the sour pre-production column height to a pure CO_2 column height. Where a pure CO_2 stream is injected into a sour gas reservoir, we can expect larger column heights of CO_2 than would have been predicted using the pure methane IFT for the initial gas in place, again assuming that the capillary entry pressure of the seal was the limiting factor in determining the pre-production column height.

4.2.2 Case (ii): A sour CO_2 stream is injected in a field that did not initially contain sour gas

This is the simplest case to consider. The IFT of a CO_2+H_2S injection mixture, with a known composition, can be calculated using Eqn 10. This IFT can then be used to find the column height conversion factor Eqn 7 and estimate the new column height. The estimated maximum CO_2 column height will be reduced compared to injecting pure CO_2, again assuming that the capillary entry pressure of the seal was the limiting factor in determining the pre-production column height.

4.2.3 Case (iii): Where a sour CO_2 stream is injected into a sour gas reservoir

Here we need to estimate both the injected sour CO_2 IFT and the produced sour gas IFT. The magnitude of the ratio of these IFTs will determine whether there will be a net increase or decrease in column height compared to non-sour case. The calculation of the IFT relies on knowing the mole fraction of each component, which must be assessed on a case-by-case basis.

Here we present one specific case to demonstrate the non-linear trend in IFT ratio with depth that emerges as a consequence of the non-linear equations of state. We consider the case where we extract H_2S from a produced gas and 100 % of this H_2S is re-injected within the injection gas, and assuming 100 % efficient volume for volume replacement of total gas within the reservoir; this conserves the molar concentration of H_2S. The produced gas is composed purely of CH_4 and H_2S. First we need to calculate the total number of moles per unit volume of H_2S in the produced gas under reservoir conditions,

$$m_{H_2S}^{produced} = \frac{m_{CH_4}^{produced} x_{H_2S}^{produced}}{1 - x_{H_2S}^{produced}} \approx \frac{x_{H_2S}^{produced}}{1 - x_{H_2S}^{produced}} \frac{\rho_{CH_4}^{subsurface}}{M_{CH_4}}, \qquad (11)$$

The injection stream is a single phase composed purely of CO_2 and H_2S and is assumed to have the same number of moles of H_2S per unit volume under reservoir conditions as were present in the produced gas, so that 100 % of the produced H_2S is

re-injected. Assuming any density change in the injection stream due to the presence of H_2S is negligible, the mole fraction of H_2S in the injection stream can be calculated

$$x_{H_2S}^{injected} = \frac{m_{H_2S}^{produced}}{m_{H_2S}^{produced} + m_{CO_2}} \approx \frac{m_{H_2S}^{produced}}{m_{H_2S}^{produced} + \frac{\rho_{CO_2}^{subsurface}}{M_{CO_2}}} . \quad (12)$$

These two equations are non-linearly related due to the effect of the density of CO_2 and CH_4 at reservoir pressure and temperature. In figure 4 we explore this non-linear relation as a function of depth using the two scenarios presented earlier in Figure 2 to define the subsurface pressure and temperature trends.

We calculate the mole fraction of H_2S in the injection stream for mole fractions in the produced gas of 0.01, 0.02, 0.05 and 0.1 using Eqns (11) and (12) over 2 km depth range. These are plotted in Figure 4a where the diagonal dashed lines show lines of equivalence between gas compositions where $IFT^{subsurface}{}_{produced} = IFT^{subsurface}{}_{injected}$ in black and $IFT^{subsurface}{}_{produced} = 2\ IFT^{subsurface}{}_{injected}$ in red; the latter being equivalent to the non sour case presented earlier in this paper where the IFT of pure CO_2 was noted to be half that of pure CH_4 which is confirmed by this line of equivalence passing through the origin where there is no H_2S in either stream.

In the inset in Figures 4a and b we zoom in on the data and add contours of constant depth. In both cases the mole fraction in the injection stream initially decreases with depth before increasing again, reflecting the trade off in density variations between CO_2 and methane with depth (Figure 1). This is shown more clearly in Figures 4c and d where the mole fraction of H_2S in the injection stream is plotted as a function of depth (solid line) compared to the mole fraction of H_2S in the produced gas (dashed line) for the same range of H_2S contents in the produced gas.

Having calculated the mole fraction of H_2S in both the produced and injected streams as a function of depth, we can use Eqn 10 to find the ratio of the IFTs in the injected and produced gasses, which is required to determine the column height conversion factor (Eqn 7). In this example, mole for mole conservation of H_2S in the produced and injection streams assuming a total volume for volume replacement of the gasses produces a weak increase in the IFT ratio tending to increase column heights.

Note that the case of large proportions of H_2S requires a full calculation of the density of the mixture, which remains beyond the scope of this paper. We have not

considered the modifications to the phase diagram associated with multi-component gasses, such as the change in bubble point because such a complete treatment is non-unique and substantially beyond the scope of this paper; the concepts outlined here remain pertinent to the full analysis.

5 Conclusions

We have demonstrated the utility of a simple conversion factor to estimate safe CO_2 column heights in depleted gas fields from known, pre-production gas column heights. This technique has greater utility than estimation from first principles, as pore throat radii do not need to be estimated, a procedure which would introduce order of magnitude uncertainties. The measurement of this property requires specific core which may not be available. The conversion factor takes into account the differences in buoyancy drive, interfacial tensions and contact angles between the two systems.

Where CO_2 is in the dense phase, the reduction in capillary entry pressure as a consequence of interfacial tension differences at the seal is at least balanced by the decrease in buoyancy of supercritical CO_2 compared to natural gas. Thus actual reductions in the column height are then derived from changes in contact angles, about which there are large theoretical and experimental uncertainties.

Neglecting the role of contact angles, an optimistic approach, for fields with CO_2 in the dense phase, typical conversion factors are in the range of 1.0-2.0 for the UK Southern North Sea case studies. For shallow-buried fields with low pressure CO_2 in the gas phase, the column height conversion factor can be as low as 0.5.

A more conservative estimate includes an assessment of fluid-mineral contact angle ratios, about which there is significant uncertainty but is a number less than but on the order of 1. For shaley caprocks this may be as low as 0.7, but this endmember estimate was based on a single mineral analysis and scaling up to a complex reservoir caprock is likely to increase this number towards 1 as suggested by other studies. For example, experiments on carbonate rich caprocks indicate that caprock will remain water wet. Taking the most extreme value for the single mineral reduces conversion factors to between 0.7-1.3 for the Southern North Sea case studies. This suggests that more research should be directed towards understanding wetting behaviour in CO_2-rich systems to determine whether wettability is a significant control in real systems.

Acknowledgements

M. Naylor is funded by the Scottish Government and the Royal Society of Edinburgh. M. Wilkinson was funded by the UKERC.

Variable Glossary

P	Reservoir pressure [MPa]
T	Reservoir temperature [K]
S_g	The specific gravity
B_{gas}	The gas formation factor
Z_{gas}	Compressibility of produced gas
w_s	Weight percent of dissolved salt in formation water
m_y	Molar concentration of component y [mol/m^3]
x_y	Mole fraction of component y in a mixture
$\psi_{gas/CO2}$	Natural gas to CO2 column height conversion factor
$\rho_w, \rho_{gas}, \rho_{CO2}$	Density of formation water, produced gas, carbon dioxide [kg/m^3]
$\Delta\rho_{X/Y}$	Density difference between substances Y and X [kg/m^3]
$\gamma_{X/Y}$	Interfacial tension between substances X and Y
$\cos\ \theta_{X/Y}$	Contact angle for substances X and Y on some implicit solid matrix
$h_{X/Y}$	Column height of substance X with substance Y above
M_y	Molecular weight of component y [g/mol]
r_p	Pore radius
r_t	Throat radius
$R_{gas} = 8.3144E-3$	Universal gas constant for P and T in [MPa] and [K]

Appendices

Formation water density, ρ_w

All of the calculations in this section are using T[F], P[psia] and density[lbm/ft^3] as described by Danesh [2007]. The resulting density, ρ_w needs to be converted back into SI units to integrate with the rest of the analysis.

The formation water density at standard conditions expressed in the weight percent of dissolved salt, w_s can be estimated in the form,

$$\rho_{w(standard)} = 62.368 + 0.438603 w_s + 1.60074 \times 10^{-3} w_s^{\,2}.$$

Neglecting the mass of dissolved gas in the water at reservoir conditions, the water density at reservoir conditions can be calculated as,

$$\rho_w = \frac{\rho_{w(standard)}}{B_w} \quad .$$

Where B_w is the formation water volume factor at standard conditions which can be calculated knowing the reservoir P and T (McCain, 25).

$$B_w = (1 + \Delta V_{w,P})(1 + \Delta V_{w,T})$$

This expression contains a pressure and temperature correction factor,

$$\Delta V_{w,P} = -P(3.58922E-7 + 1.95301E-9T) - P^2(2.25341E-10 + 1.72834E-13T)$$

$$\Delta V_{w,T} = -1.001E-2 + 1.33391E-4T + 5.50654E-7T^2$$

Produced gas density (dry gas), ρ_{gas}

Using the ideal gas formula the density under reservoir conditions [*A Danesh*, 2007] is expressed as,

$$\rho_{gas} = \frac{PM_{gas}}{Z_{gas} R_{gas} T}$$

Where,

The gas formation factor, B_{gas} describes the ratio of the gas volume at reservoir conditions compared to the gas volume at standard conditions and is frequently a recorded reservoir parameter. This can be used to the compressibility of the gas,

$$Z_{gas} = \frac{B_{gas} P}{3.47 \times 10^{-4}\ T} \quad .$$

Where the molecular weight is known, this can be used directly. For pure methane, $M_{gas} = 16$. For natural gas mixtures it will be higher, typically ~22 [*R C Selley*, 1998]. For gasses with heavier hydrocarbon molecules, such as pentane, it can be as high as ~43 (Kapuni field, NZ [*R C Selley*, 1998]).

The specific gravity is often the quoted parameter, which relates the molecular weight of gas at standard conditions to the molecular weight of air at standard conditions, $M_{gas} = S_g M_{air} = 28.96 S_g$.

References

Abbotts, I. L. (1991), *United Kingdom Oil and Gas Fields 25 Years Commemorative Volume*.

Aggelopoulos, C. A, Robin, M, Perfetti, E, Vizika, O (2010) CO2/CaCl2 solution interfacial tensions under CO2 geological storage conditions: Influence of cation valence on interfacial tension. *Advances in Water Resources* vol. 33 (6) pp. 691-697

Bachu, S., and J. Shaw (2003), Evaluation of the CO2 sequestration capacity in Alberta's oil and gas reservoirs at depletion and the effect of underlying aquifers, *Journal of Canadian Petroleum Technology*, *42*(9), 51-61.

Berg, R. R. (1975), Capillary Pressures in Stratigraphic Traps, *Aapg Bulletin-American Association of Petroleum Geologists*, *59*(6), 939-956.

Bloch, S. (1991), Empirical prediction of porosity and permeability in sandstones, *AAPG Bulletin*, *75*, 1145–1160.

S., Brown (1984) Jurassic in: K.W. Glennie (Ed.) Introduction to Petroleum Geology of the North Sea, Wiley-Blackwell

Cai, B.Y., Yang, J.T. and Guoet, T.M. (1996) Interfacial tension of hydrocarbon+ water/brine systems under high pressure. *J. Chem. Eng. Data* vol. 41 (3) pp. 493-496

Chalbaud, C., M. Robin, J-M Lombard, F. Martin, P. Egermann, and H. Bertin, Interfacial tension measurements and wettability evaluation for geological CO2 storage *Advances in Water Resources* 32 (1) 98-109 doi:10.1016/j.advwatres.2008.10.012

Chiquet, P., D. Broseta, and S. Thibeau (2007a), Wettability alteration of caprock minerals by carbon dioxide, *Geofluids*, *7*(2), 112-122.

Chiquet, P., J. L. Daridon, D. Broseta, and S. Thibeau (2007b), CO2/water interfacial tensions under pressure and temperature conditions of CO2 geological storage, *Energy Conversion and Management*, *48*(3), 736-744.

Danesh, A. (2007), *PVT and phase behaviour of petroleum reservoir fluids*, Elsevier.

Espinoza, D. N., and Santamarina J.C., (2010) Water-CO2-mineral systems: Interfacial tension, contact angle, and diffusion-Implications to CO2 geological storage. Water Resour Res vol. 46 pp. W07537

Hildenbrand, A., S. Schlomer, B. M. Krooss, and R. Littke (2004), Gas breakthrough experiments on pelitic rocks: comparative study with N-2, CO2 and CH4, *Geofluids*, *4*(1), 61-80.

Li, S., M. Dong, Z. Li, S. Huang, H. Qing, and E. Nickel (2005), Gas breakthrough pressure for hydrocarbon reservoir seal rocks: implications for the security of long-term CO2 storage in the Weyburn field, *Geofluids*, *5*(4), 326-334.

Li, Z. W., M. Z. Dong, S. L. Li, and S. Huang (2006), CO2 sequestration in depleted oil and gas reservoirs - caprock characterization and storage capacity, *Energy Conversion and Management*, *47*(11-12), 1372-1382.

Massoudi, R. and King, A.D. (1975) Effect of pressure on surface-tension of aqueous-solutions - adsorption of hydrocarbon gases, carbon-dioxide, and nitrous-oxide on aqueous-solutions of sodium-chloride and tetra-normal-butylammonium bromide at 25 degrees. *J Phys Chem-Us* vol. 79 (16) pp. 1670-1675

Moss, B., Barson, D., Rakhit, K., Dennis, H. & Swarbrick, R., (2003) Formation pore pressures and formation waters. In: Evans, D., Graham, C., Armour, A. & Bathurst, P. (eds) *The Millennium Atlas: Petroleum Geology of the Central and Northern North Sea*. Geological Society, London. p. 317-329

Ren, Q. Y., G. J. Chen, W. Yan, and T. M. Guo (2000), Interfacial Tension of (CO2+CH4) plus water from 298 K to 373 K and pressures up to 30 MPa, *J. Chem. Eng. Data*, *45*(4), 610-612.

Rezaee, M. R., A. Jafari, and E. Kazemzadeh (2006), Relationships between permeability, porosity and pore throat size in carbonate rocks using regression analysis and neural networks, *Journal of Geophysics and Engineering*(4), 370.

Selley, R. C. (1998), *Elements of Petroleum Geology*, Academic Press.

Shah, V., Broseta, D., and Mouronval, G., (2008a) Capillary alteration of caprocks with acid gases. SPE paper 113353, presented at the 2008 SPE IOR Symposium, Tulsa.

Shah, V., Droseta, D., Mouronval, G. and Montel, F. (2008b) Water/acid gas interfacial tensions and their impact on acid gas storage, *International Journal of Greenhouse Gas Control* 2, 594-604

Stouffer, C.E., Kellerman, S.J., Hall, K.R., Holste, J.C., Gammon, B.E. and Marsh, K.N. (2001) Densities of carbon dioxide plus hydrogen sulfide mixtures from 220 K to 450 K at pressures up to 25 MPa. *J Chem Eng Data* vol. 46 (5) pp. 1309-1318

Tonnet, N., Broseta, D. and Mouronval, G. (2010) Evaluation of the petrophysical properties of a carbonate-rich caprock for CO_2 geological storage purposes, SPE 131525.

Yang, D.Y., Gu, Y.A., and Tontiwachwuthikul, P. (2008) Wettability determination of the crude oil-reservoir brine-reservoir rock system with dissolution of CO_2 at high pressures and elevated temperatures, *Energy and Fuels* 22 (4), 2362-2371

Yang, D.Y., Tontiwachwuthikul, P. and Gu, Y.G. (2005) Interfacial tensions of the crude oil plus reservoir brine + CO_2 systems at pressures up to 31 MPa and temperatures of 27 degrees C and 58 degrees C Journal of Chemical and Engineering Data, 50 (4), 1242-1249, doi: 10.1021/je0500227

Tables

Table 1- Calculated column height ratios for gas fields from the UK Southern North Sea.

Field name	Pressure [MPa]	Temp [K]	CO_2 Density [kg/m^3]	Corrected water density [kg/m^3]	Gas expansion factor	Gas compressibility	Molecular Weight of Gas	Gas density [kg/m^3]	CO_2/water density difference [kg/m^3]	Gas/water density difference [kg/m^3]	Density ratio	IFT Ratio	Maximal column Height correction factor	Safe column Height correction factor
Amythest	28.25	360.93	692.54	1149.79	235.0	0.960	16.962	166.361	457.25	983.42	2.15	0.502	1.079	0.755
Barque	26.53	352.59	709.30	1123.00	229.0	0.947	16.650	159.126	413.70	963.87	2.33	0.501	1.167	0.817
Camelot	19.64	338.71	681.60	1113.31	192.0	0.870	16.915	135.539	431.71	977.77	2.26	0.500	1.133	0.793
Cleeton	28.58	352.59	733.50	1250.30	244.0	0.957	16.975	172.857	516.80	1077.44	2.08	0.501	1.045	0.731
Clipper	26.53	352.59	709.20	1123.38	229.0	0.947	16.535	158.027	414.18	965.36	2.33	0.501	1.168	0.818
Leman	20.82	324.82	785.30	1169.40	229.0	0.807	16.667	159.293	384.10	1010.11	2.63	0.501	1.318	0.922
Ravenspurn S	30.94	366.48	699.20	1239.46	240.0	1.014	16.932	169.600	540.26	1069.86	1.98	0.502	0.995	0.696
Rough	31.23	364.82	709.30	1223.43	255.5	0.966	17.010	181.384	514.13	1042.05	2.03	0.502	1.016	0.712
Sean S	58.57	362.04	887.30	1158.40	192.0	2.428	17.209	137.896	271.10	1020.51	3.76	0.503	1.894	1.326
Sean N	58.57	367.59	872.80	1154.84	202.0	2.273	17.005	143.356	282.04	1011.49	3.59	0.502	1.800	1.260
West Sole	29.39	358.15	717.60	1152.21	239.0	0.989	16.787	167.441	434.61	984.77	2.27	0.502	1.137	0.796

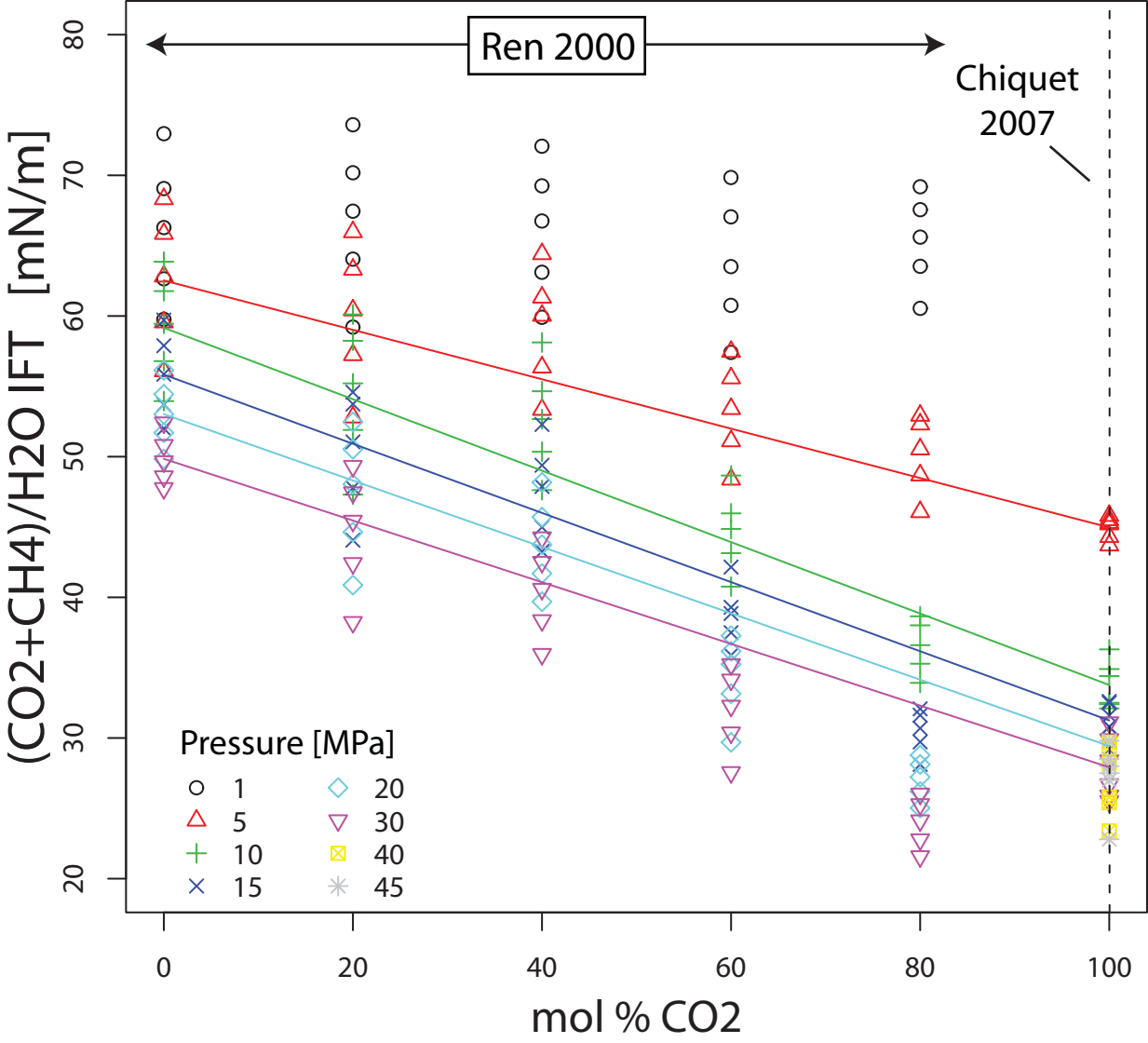
Ren 2000
Chiquet 2007
(CO2+CH4)/H2O IFT [mN/m]
mol % CO2
Pressure [MPa]
1
5
10
15
20
30
40
45
20
30
40
50
60
70
80
0
20
40
60
80
100

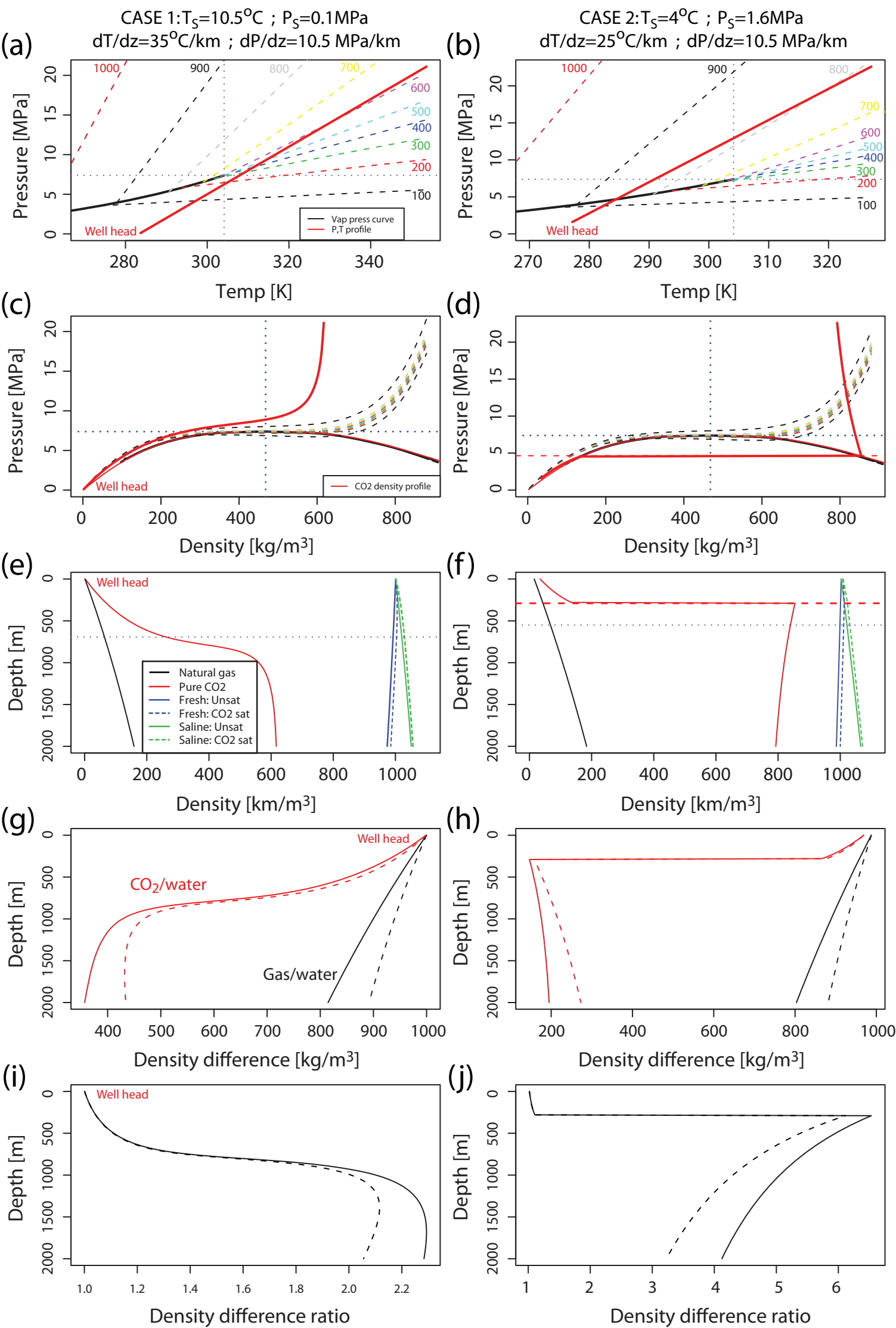
CASE 1:T$_S$=10.5°C ; P$_S$=0.1MPa
dT/dz=35°C/km ; dP/dz=10.5 MPa/km
CASE 2:T$_S$=4°C ; P$_S$=1.6MPa
dT/dz=25°C/km ; dP/dz=10.5 MPa/km
(a)
(b)
(c)
(d)
(e)
(f)
(g)
(h)
(i)
(j)
Pressure [MPa]
Temp [K]
Density [kg/m3]
Depth [m]
Density difference [kg/m3]
Density difference ratio
Well head
1000
900
800
700
600
500
400
300
200
100
Vap press curve
P,T profile
CO2 density profile
Natural gas
Pure CO2
Fresh: Unsat
Fresh: CO2 sat
Saline: Unsat
Saline: CO2 sat
CO2/water
Gas/water

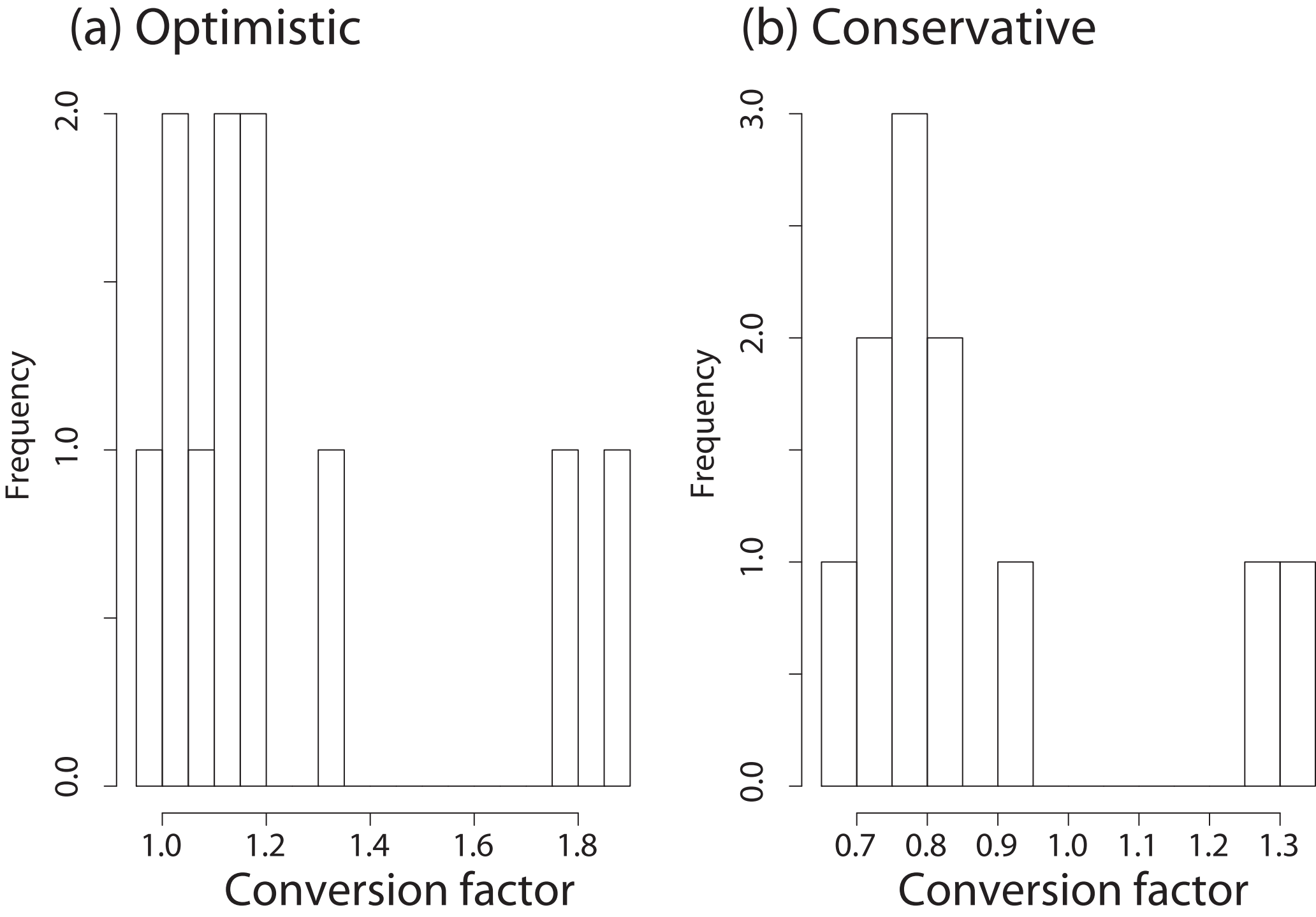
(a) Optimistic
Frequency
0.0
1.0
2.0
1.0
1.2
1.4
1.6
1.8
Conversion factor
(b) Conservative
Frequency
0.0
1.0
2.0
3.0
0.7
0.8
0.9
1.0
1.1
1.2
1.3
Conversion factor

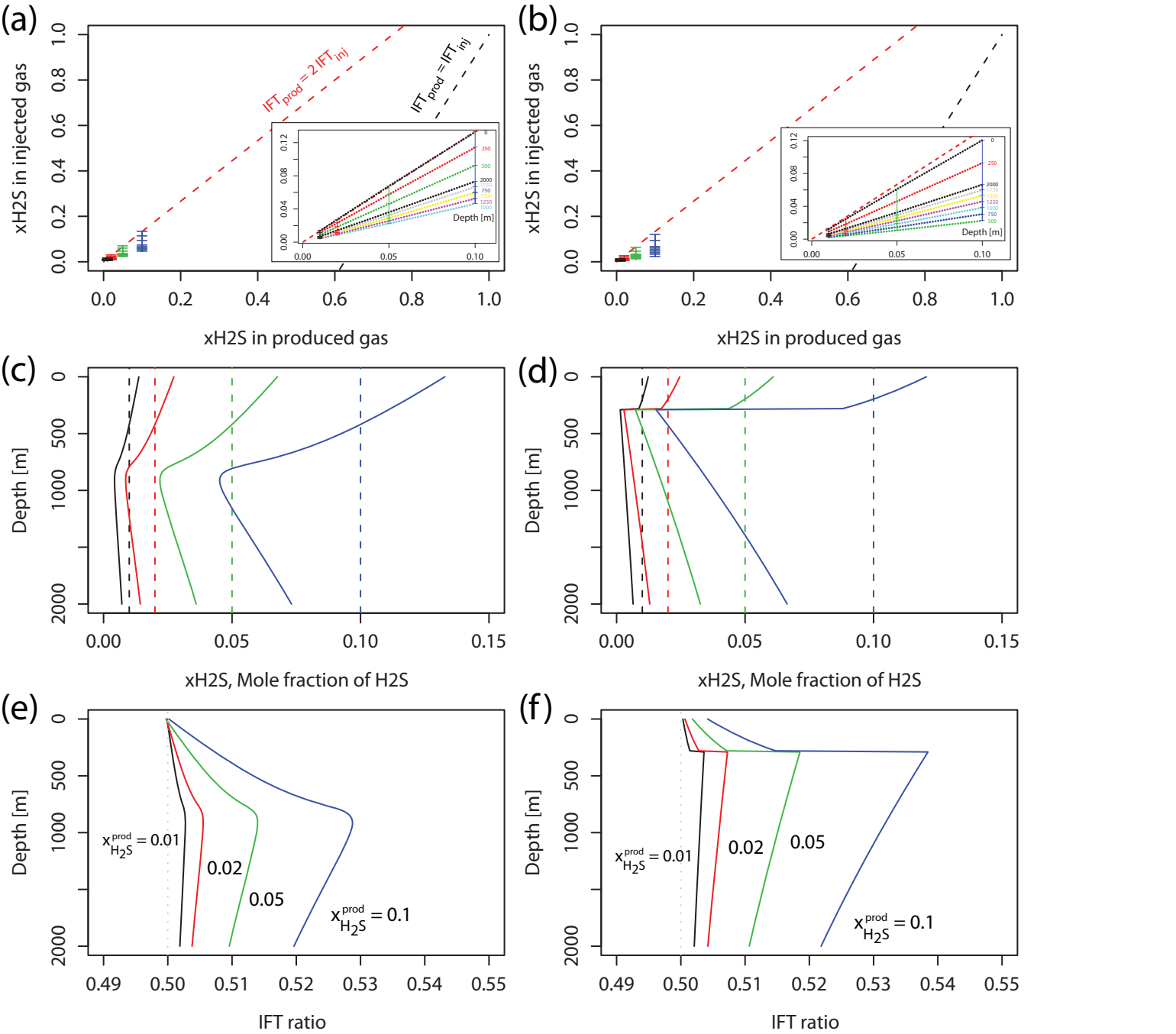
(a)
(b)
(c)
(d)
(e)
(f)
xH2S in injected gas
xH2S in produced gas
IFT_prod = 2 IFT_inj
IFT_prod = IFT_inj
Depth [m]
xH2S, Mole fraction of H2S
IFT ratio
x_H2S^prod = 0.01
0.02
0.05
x_H2S^prod = 0.1

Figure captions

Figure 1 (Colour online) Compilation of IFT data for (CO_2+CH_4)/water mixtures [*Q Y Ren et al.*, 2000] and for the pure CO_2/water [*P Chiquet et al.*, 2007b]. For the data between 0 to 80 mol%CO_2, at each pressure measurements are taken at 4 temperatures (298.15K, 313.15K, 333.15K, 353.15K and 373.15K). For the data at 100 mol%CO_2, measurements were taken at 5 different temperatures. Chiquet suggested that previous measurements of IFT were biased to lower values because they assumed a density of the CO_2 saturated water that proved inaccurate; we interpret it as being likely that the IFT values for the CO_2+CH_4 mixtures lie closer to the lines fitted between the pure CO_2 and pure CH4 IFT values. This interpretation is supported by the tight clustering of the Chiquet measurements compared to Ren.

Figure 2 (Color online) Phase properties and buoyancy drives for two different subsurface scenarios. The left hand figures refer to a sub-aerial case and the right a submarine case. (a,b) Vapour pressure curves (solid black) with subsurface pressure temperature trajectory (solid red). Contours of constant density as a function of pressure and temperature have been added in dashed lines; the corresponding density [kg/m^3] has been written in the same color. Dotted blue lines are the critical pressure and temperature. (c,d) Subsurface densities (solid red line) plotted on a pressure-density phase diagram. The black solid line shows the saturated vapour curve and the dew point curve. Some isotherms have been added near the critical point for reference as dashed lines. Dotted blue lines show the critical density and pressure. The dashed red line in (d) is the phase change pressure. (e,f) Natural gas, CO_2, fresh water and saline density profiles. The blue dotted line is the depth corresponding to the critical pressure and the red dashed line in (f) is the depth at which the phase change occurs.

(g,h) Density differences between the (1) natural gas and fresh water (black solid) or saline (black dashed) (2) CO_2 and fresh water (red solid) or saline (red dashed). (i,j) Density difference ratios between (1) gas/fresh water and CO_2/fresh water systems (solid lines) and (2) gas/saline and CO_2/saline systems (dashed lines).

Figure 3 Histogram of (a) maximal and (b) safe (including experimental contact angle data) column height ratios for the Southern North Sea dataset described in the text.

Figure 4 (Color online) Generalisation to acid gases. Here we present an evaluation of the impact of H_2S on the interfactial tension ratio assuming the same molarity of H_2S in a produced methane stream and in an injected CO_2 stream. (a,b) Plot showing the produced and injected molar fractions of H_2S. The line of equivalence where the gas compositions have the same IFT is shown with the black dashed line. The line of equivalence where the injected (CO_2+H_2S) stream has half the IFT of the produced (CH_4+H_2S) gas is shown with the red dashed line. Calculations have been performed to calculate the molar fraction of H_2S in the injection stream assuming a constant molar fraction in the produced gas as a function of depth. The inset figure zooms in on the data and adds contours of depth. Note how the injected molar fraction decreases with depth then increases again. (c,d) Plot of the molar fraction of H_2S in the injection stream (solid line) given some molar fraction in the produced gas (dashed line). The molar fractions vary non-linearly as they are dependent upon the densities of the CO_2 and methane which vary non-linearly with depth (Figure 2c,d). (e,f) The IFT ratio is calculated as a function of depth using Eqn 10. The IFT of the injection stream is always slightly greater than half the IFT of the produced gas. These ratios also vary non-linearly with depth because they are functions of the molar fractions.